Journal of Solid State Chemistry **156,** 464–469 (2001)
doi:10.1006/jssc.2000.9025, available online at http://www.idealibrary.com on IDEAL®

Spin Dimer Analysis for Antiferromagnetic Spin Exchange Interactions of Magnetic Solids with Several Unpaired Electrons per Spin Site: Trends in the Spin Exchange Parameters of the Compounds Consisting of MnF_5 Chains and CrX_2 (X = O, S) Layers

H.-J. Koo and M.-H. Whangbo[1]

Department of Chemistry, North Carolina State University, Raleigh, North Carolina 27695-8204,

and

S. Coste and S. Jobic[1]

Institut des Matériaux Jean Rouxel, Laboratoire de Chimie des Solides, 2 rue de la Houssinière, B.P. 32229, 44322 Nantes Cedex 03, France

Received July 17, 2000; in revised form October 18, 2000; accepted November 6, 2000, published online December 21, 2000

For magnetic solids with several unpaired spins per spin site, the average spin orbital interaction energies $\langle \Delta e \rangle$ and the average spin orbital interaction energy squares $\langle (\Delta e)^2 \rangle$ were defined as a qualitative measure for the strengths of their antiferromagnetic spin exchange interactions. The trends in the antiferromagnetic spin exchange interactions of the magnetic solids containing MnF_5 chains and CrX_2 (X = O, S) layers were examined in terms of the $\langle \Delta e \rangle$ and $\langle (\Delta e)^2 \rangle$ values calculated for their spin dimers. © 2001 Academic Press

1. INTRODUCTION

Recently it has been shown (1–7) that trends in the antiferromagnetic spin exchange interactions of magnetic solids containing Cu^{2+} (d^9) and V^{4+} (d^1) cations are well described by the spin orbital interaction energies calculated for their spin dimers (i.e., the structural units containing two adjacent spin sites). These compounds possess only one unpaired spin per spin site, so their spin exchange interactions are considerably simpler to describe than are those of magnetic solids with several unpaired spins per spin site (8). In the present work we probe how antiferromagnetic spin exchange interactions of magnetic solids with several unpaired spins per spin site are related to their crystal structures based on the spin orbital interaction energies calculated for their spin dimers. As representative examples of such magnetic solids, we consider the compounds consisting of MnF_5 chains (9–22) and those containing CrX_2 (X = O, S) layers (23–33), which contain high-spin Mn^{3+} (d^4) and Cr^{3+} (d^3) cations, respectively.

[1]To whom the correspondence should be addressed.

2. SPIN EXCHANGE INTERACTIONS AND SPIN DIMERS

$A_2MnF_5 \cdot H_2O$ (A = K, Rb, Cs, Tl), $A'MnF_5 \cdot H_2O$ (A' = Sr, Ba), and A_2MnF_5 (A = Li, Na, NH_4, Rb, Cs) contain MnF_5 chains made up of corner-sharing MnF_6 octahedra (Fig. 1) (9–22). Each Mn^{3+} cation of these compounds is in a high-spin state and therefore has four unpaired spins. The spin monomers (i.e., the structural units containing a spin site) and spin dimers of these compounds are given by $(MnF_6)^{3-}$ and $(Mn_2F_{11})^{5-}$ clusters, respectively (Figs. 2a and 2b). With one electron in the e_g-block levels, each $(MnF_6)^{3-}$ octahedron undergoes a Jahn–Teller distortion such that with respect to the local Cartesian coordinate system chosen in Fig. 2a, the two axial Mn–F bonds aligned along the z-axis ($Mn–F_{ax}$) become longer than the four equatorial Mn–F bonds ($Mn–F_{eq}$). Thus in the d-block levels of a distorted $(MnF_6)^{3-}$ octahedron, the $x^2–y^2$ level is empty while the remaining d-levels are each singly filled (Fig. 2c). In all the MnF_5-chain containing compounds, the intrachain spin exchange interactions are antiferromagnetic (16). The bond angles of the $Mn–F_{ax}–Mn$ bridges and the intrachain spin exchange parameters J of the MnF_5-chain containing compounds are listed in Table 1. As already pointed out (16), the magnitude of the intrachain spin exchange parameter J generally increases with increasing the $\angle Mn–F_{ax}–Mn$ angle toward 180° (Fig. 3). In general, the

0022-4596/01 $35.00

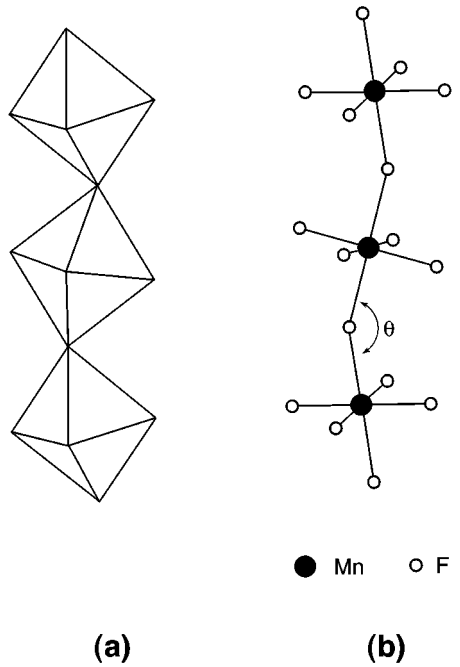

FIG. 1. Schematic diagrams of a MnF_5 chain present in $A_2MnF_5 \cdot H_2O$ (A = K, Rb, Cs, Tl), A'Mn $F_5 \cdot H_2O$ (A' = Sr, Ba), and A_2MnF_5 (A = Li, Na, NH_4, Rb, Cs). (a) Polyhedral representation and (b) ball-and-stick representation. In general, the $\angle$ Mn–F_{ax}–Mn angle, θ, is close to 180° for large cations A and becomes smaller as the cation size decreases.

TABLE 1

Mn–F_{ax}–Mn Bridge Angles θ, Spin Exchange Parameters J, $\langle \Delta e \rangle$, and $\langle (\Delta e)^2 \rangle$ Values of the MnF_5-Chain Containing Magnetic Solids

Compound	θ (°)	$-J/k_B$ (K)	$\langle \Delta e \rangle$ (10^{-3} eV)	$\langle (\Delta e)^2 \rangle$ (10^{-3} eV^2)
$Tl_2MnF_5 \cdot H_2O$	179.0[a]	21.5[a]	15.9	2.2
$Rb_2MnF_5 \cdot H_2O$	176.0[b]	21.8,[c] 20.5,[d] 20.0[e]	15.6	2.1
$K_2MnF_5 \cdot H_2O$	163.3[f]	18.2,[c] 15.5[d]	13.0	1.3
$Cs_2MnF_5 \cdot H_2O$	180.0[g]	19.0,[e] 17.9[c]	14.3	1.9
Rb_2MnF_5	180.0[h]	22.6[c]	16.7	2.3
Cs_2MnF_5	180.0[i]	19.4[c]	14.8	2.0
$(NH_4)_2MnF_5$	143.4[j]	11.2,[e] 10.6,[k] 10.45[d]	8.7	0.5
Na_2MnF_5	132.5[l]	9.2,[k] 8.6,[m] 8.25 [e]	3.7	0.1
Li_2MnF_5	121.5[e]	6.3,[e] 5.6[k]	5.4	0.2
$BaMnF_5 \cdot H_2O$	147.7[n]	13.5[e]	9.3	0.7
$SrMnF_5 \cdot H_2O$	139.8[n]	10.3[e]	6.9	0.3

[a]Ref. 9.
[b]Ref. 10.
[c]Ref. 11.
[d]Ref. 12.
[e]Ref. 13.
[f]Ref. 14.
[g]Ref. 15.
[h]Ref. 16.
[i]Ref. 17.
[j]Ref. 18.
[k]Ref. 19.
[l]Ref. 20.
[m]Ref. 21.
[n]Ref. 22.

$\angle$ Mn–F_{ax}–Mn angle becomes larger with increasing size, and hence the polarizing power of the countercation. A notable shortcoming of this plot is that the four compounds with strong spin exchange interactions, $Tl_2MnF_5 \cdot H_2O$, $Cs_2MnF_5 \cdot H_2O$, Rb_2MnF_5, and Cs_2MnF_5, are not clearly distinguished.

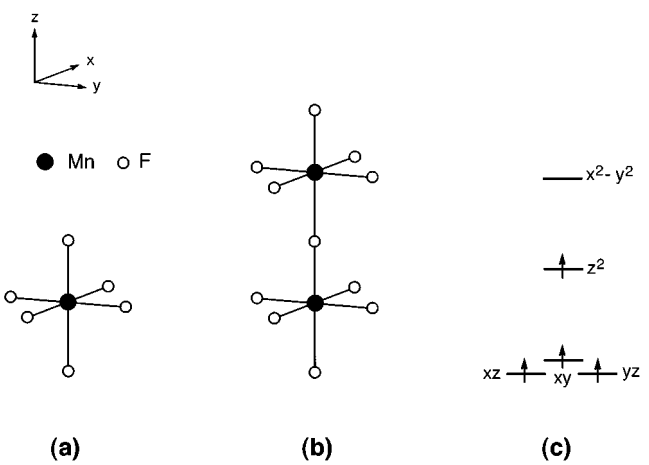

FIG. 2. Schematic representations of (a) the spin monomer $(MnF_6)^{3-}$ and (b) the spin dimer $(Mn_2F_{11})^{5-}$. For convenience, the $\angle$ Mn–F_{ax}–Mn angle was taken to be 180° in (b). The occupancy of the d-block levels of a $(MnF_6)^{3-}$ spin monomer is shown in (c).

$ACrO_2$ (A = Li, Na, K, Cu, Ag) (23–28) and $ACrS_2$ (A = Li, Na, K, Cu, Ag) (29–33) contain CrX_2 layers (X = O, S) of CdI_2 type, which are made up of edge-sharing CrX_6 octahedra (Fig. 4). Each Cr^{3+} cation of these compounds is in a high-spin state and therefore has three unpaired spins. The spin monomers and spin dimers of a CrX_2 layer are represented by $(CrX_6)^{9-}$ and $(Cr_2X_{10})^{14-}$ clusters, respectively (Figs. 5a and 5b). In the d-block levels of a slightly distorted $(CrX_6)^{9-}$ octahedron, the t_{2g} levels are each singly filled and the e_g levels are empty (Fig. 5c). The intralayer spin exchange interactions are antiferromagnetic in all $ACrO_2$ (A = Li, Na, K, Cu, Ag) (24, 27). In $ACrS_2$ the intralayer spin exchange interactions are antiferromagnetic for A = Li, Ag, and Cu (30, 32), but ferromagnetic for A = Na and K (30, 31). Table 2 lists the intralayer spin exchange parameters J and the bond angles of the Cr–X–Cr bridges in the $ACrX_2$ systems for which the intralayer spin exchange interactions are antiferromagnetic. As plotted in Fig. 6, the magnitude of the spin exchange parameter J generally decreases with increasing $\angle$ Cr–X–Cr angles.

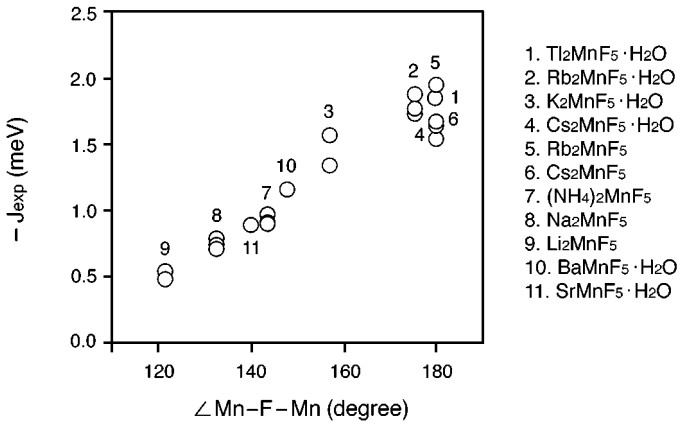

FIG. 3. Plot of the intrachain spin exchange parameter J versus the $\angle$ Mn–F_{ax}–Mn angle for the MnF_5-chain containing magnetic solids.

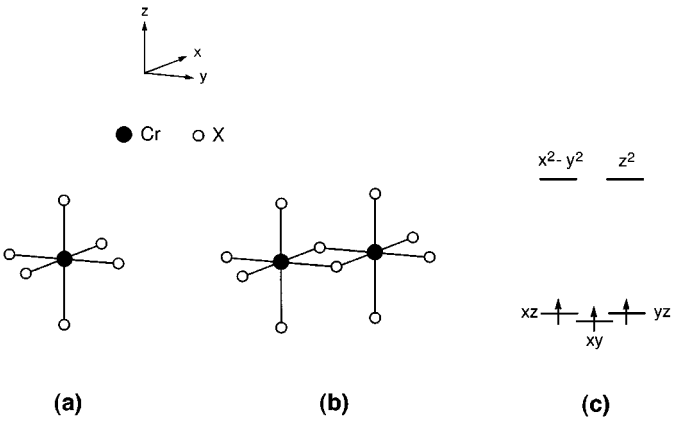

FIG. 5. Schematic representations of (a) the spin monomer $(CrX_6)^{9-}$ and (b) the spin dimer $(Cr_2X_{10})^{14-}$. The occupancy of the d-block levels of a $(CrX_6)^{9-}$ spin monomer is shown in (c).

3. AVERAGE SPIN ORBITAL INTERACTION ENERGY

The spin exchange parameter J of a spin dimer containing two unpaired spins corresponds to the energy difference ΔE between the triplet and singlet states of the spin dimer, i.e., $J = \Delta E = {}^1E - {}^3E$, where ${}^1E$ and ${}^3E$ are the total energies of the singlet and triplet states, respectively (34, 35). Quantitative evaluation of spin exchange parameters J has been a challenging task and requires state-of-the-art computational efforts based on either configuration interaction wave functions or density functional theory (DFT) (36). The J values for transition metal oxides and fluorides of perovskite-type structures are well reproduced by the ΔE values of the corresponding spin dimers determined from first principles electronic structure calculations (37). Recent DFT calculations of the intrachain J values of magnetic solids A_2MnF_5 (A = Rb, Cs, NH_4, Na, Li) are in good agreement with experiment (38).

In general the spin exchange parameter J can be expressed as $J = J_F + J_{AF}$, where the ferromagnetic term J_F favors the triplet state (i.e., $J_F > 0$), and the antiferromagnetic term J_{AF} favors the singlet state (i.e., $J_{AF} < 0$) (34, 35). Qualitative trends in the antiferromagnetic J parameters of

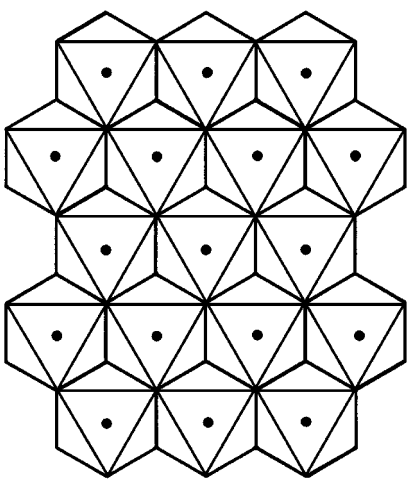

FIG. 4. Schematic projection view of a CrX_2 layer present in $ACrO_2$ and $ACrS_2$ (A = Li, Na, K, Cu, Ag) along the direction perpendicular to the layer.

TABLE 2

Cr–X–Cr Bridge Angles θ, Spin Exchange Parameters J, $\langle \Delta e \rangle$, and $\langle (\Delta e)^2 \rangle$ Values of the CrX_2 Layer Containing Magnetic Solids

Compound	θ (°)	$-J/k_B$ (K)	$\langle \Delta e \rangle$ (10^{-3} eV)	$\langle (\Delta e)^2 \rangle$ (10^{-3} eV^2)
$LiCrO_2$	94.2[a]	39 ± 1[b]	36.4	4.1
$NaCrO_2$	95.3[c]	20 ± 1[b]	30.6	2.9
$KCrO_2$	96.8[c]	12 ± 1.5[b]	25.9	2.1
$CuCrO_2$	96.6[d]	11.4[e]	30.1	3.0
$AgCrO_2$	96.6[f]	9.0[e]	29.9	2.8
$LiCrS_2$	91.6[h]	14[i]	22.4	1.6
$CuCrS_2$	92.1[j,k]	8[i]	15.9	0.8
$AgCrS_2$	94.6[j,k]	6[i]	14.7	0.9

[a]Ref. 23.
[b]Ref. 24.
[c]Ref. 25.
[d]Ref. 26.
[e]Ref. 27.
[f]Ref. 28.
[h]Ref. 29.
[i]Ref. 30.
[j]Ref. 31.
[k]The space group for $CuCrS_2$ and $AgCrS_2$ is $R3m$, while that for the other $ACrX_2$ systems is $R\bar{3}m$. Thus each spin dimer of $CuCrS_2$ and $AgCrS_2$ has two different Cr–S–Cr bridge angles (i.e., 90.8° and 93.4° for $CuCrS_2$, and 93.4° and 95.7° for $AgCrS_2$), so their average values are listed in this table and used in plotting Fig. 6.

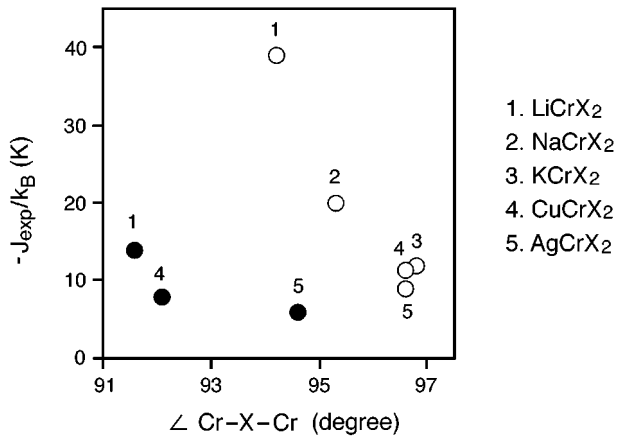

FIG. 6. Plot of the intralayer spin exchange parameter J versus the ∠Cr–Q–Cr angle for the CrX_2-chain containing magnetic solids.

magnetic solids are well explained in terms of the one-electron spin orbital interaction energies of spin dimers (1–7). The spin orbital interaction energy of a spin dimer refers to the energy difference Δe between the two singly occupied energy levels of the spin dimer when the two spin sites are equivalent (Fig. 7a) (34). For the interaction between two equivalent spins, J_{AF} is related to Δe by $J_{AF} \propto -(\Delta e)^2$ if the singly filled levels of a spin dimer are given as linear combinations of orthogonal spin orbitals at the two spin sites (34). Alternatively, J_{AF} is related to Δe by $J_{AF} \propto -S\Delta e$, when the singly filled levels of a spin-dimer are given as linear combinations of nonorthogonal spin orbitals localized at the two spin sites (35). Here S is the overlap integral between the two nonorthogonal spin orbitals. The two formulations are identical in nature due to the relationship $\Delta e \propto S$.

The spin exchange interaction of a spin dimer becomes more complicated when there are several unpaired spins per spin site (8). Provided that the spin sites A and B of a spin dimer have n_A and n_B unpaired spins, respectively, the overall spin exchange parameter J of the spin dimer is described by (8).

$$J = \sum_{\mu=1}^{n_A} \sum_{\nu=1}^{n_B} \frac{J_{\mu\nu}}{n_A n_B}. \quad [1]$$

Here $n_A = n_B = 4$ for the $(Mn_2F_{11})^{5-}$ spin dimers, and $n_A = n_B = 3$ for the $(Cr_2X_{10})^{14-}$ spin dimers. Thus, for each spin dimer, Eq. [1] has n_A diagonal terms $J_{\mu\mu}$ and $n_A(n_A - 1)$ off-diagonal terms $J_{\mu\nu}$ ($\mu \neq \nu$). One-electron molecular orbital calculations for a spin dimer provide information about how each d-level of a spin dimer splits as a result of interaction between spin sites and hence give the spin orbital interaction energies Δe associated with the n_A diagonal terms. From the viewpoint of nonorthogonal spin orbitals localized at spin sites, the antiferromagnetic contribution J_{AF} from each off-diagonal term $J_{\mu\nu}$ ($\mu \neq \nu$) are negligible because the overlap integral between two adjacent spin orbitals of different symmetry is either zero or negligible. Consequently, for the discussion of antiferromagnetic spin exchange interactions, it is reasonable to assume that only the n_A diagonal $J_{\mu\mu}$ terms can contribute significantly to the antiferromagnetic term J_{AF}; i.e.,

$$J_{AF} = \sum_{\mu=1}^{n_A} \frac{J_{\mu\mu}}{(n_A)^2}. \quad [2]$$

Therefore it would be interesting to correlate the trends in the antiferromagnetic spin exchange parameters J with the average of the spin orbital interaction energies $\langle \Delta e \rangle$ or that

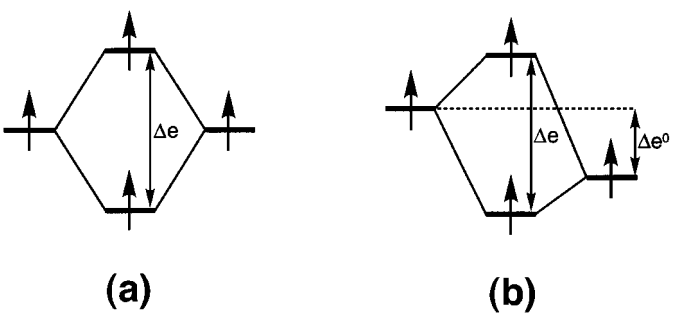

FIG. 7. Spin orbital interactions (a) between equivalent spin monomers and (b) between nonequivalent spin monomers.

TABLE 3

Exponents ξ_i and Valence Shell Ionization Potentials H_{ii} of Slater-Type Orbitals χ_i Used for Extended Hückel Tight-Binding Calculations[a]

Atom	χ_i	H_{ii} (eV)	ζ_i	c_1[b]	$\zeta_{i'}$	c_2[b]
Cr	4*s*	−8.66	1.772	1.0		
Cr	4*p*	−5.24	1.300	1.0		
Cr	3*d*	−11.2	5.410	0.3830	2.340	0.7367
Mn	4*s*	−9.75	1.844	1.0		
Mn	4*p*	−5.89	1.350	1.0		
Mn	3*d*	−11.7	5.767	0.3898	2.510	0.7297
O	2*s*	−32.3	2.688	0.7076	1.675	0.3745
O	2*p*	−14.8	3.694	0.3322	1.659	0.7448
F	2*s*	−40.0	3.136	0.6737	1.945	0.4144
F	2*p*	−18.1	4.184	0.3546	1.851	0.7299
S	3*s*	−20.0	2.662	0.5564	1.688	0.4873
S	3*p*	−13.3	2.338	0.5213	1.333	0.5443

[a] H_{ii}'s are the diagonal matrix elements $\langle \chi_i | H^{eff} | \chi_i \rangle$, where H^{eff} is the effective Hamiltonian. In our calculations of the off-diagonal matrix elements $H^{eff} = \langle \chi_i | H^{eff} | \chi_j \rangle$, the weighted formula was used. See J. Ammeter, H.-B. Bürgi, J. Thibeault, and R. Hoffmann, *J. Am. Chem. Soc.* **100,** 3686 (1978).

[b] Contraction coefficients used in the double-zeta Slater-type orbital.

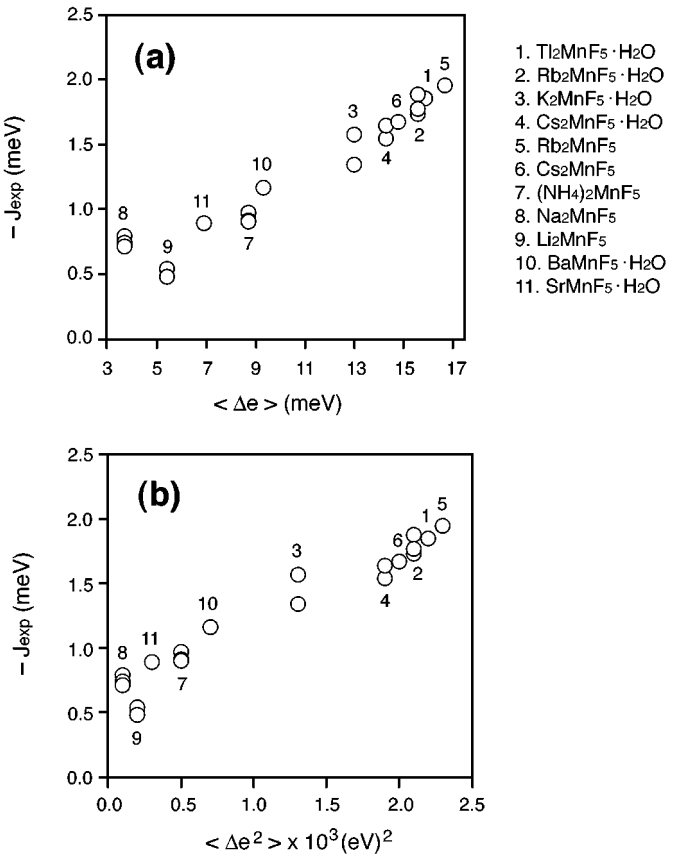

FIG. 8. Plots of (a) the intrachain J versus $\langle \Delta e \rangle$ and (b) the intrachain J versus $\langle (\Delta e)^2 \rangle$ for the MnF_5-chain compounds.

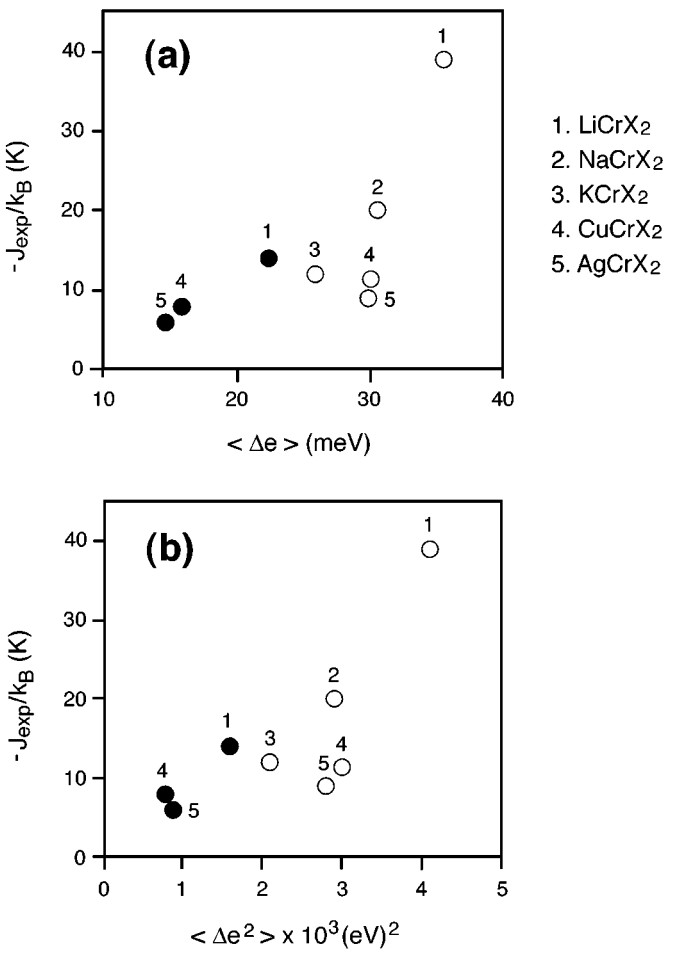

FIG. 9. Plots of (a) the intrachain J versus $\langle \Delta e \rangle$ and (b) the intrachain J versus $\langle (\Delta e)^2 \rangle$ for the CrX_2-layer compounds. The open circles represent the oxides $ACrO_2$, and the filled circles the sulfides $ACrS_2$.

of the spin orbital interaction energy squares $\langle (\Delta e)^2 \rangle$,

$$\langle \Delta e \rangle = \sum_{\mu=1}^{n_A} \frac{\Delta e_{\mu\mu}}{(n_A)^2} \qquad [3a]$$

$$\langle (\Delta e)^2 \rangle = \sum_{\mu=1}^{n_A} \frac{(\Delta e_{\mu\mu})^2}{(n_A)^2}, \qquad [3b]$$

where $\Delta e_{\mu\mu}$ refers to the spin orbital interaction energy associated with the two singly filled molecular orbitals of a spin dimer that result from the spin orbitals μ from the two spin sites (e.g., $\mu = xz$, yz, xy, z^2 for the MnF_5 chains and $\mu = xz$, yz, xy for the CrX_2 layers according to the local Cartesian systems adopted in Figs. 2a and 5a, respectively). For cases when the two spin sites are not equivalent (Fig. 7b) (39), the energy term $\Delta e_{\mu\mu}$ of Eq. [3] should be replaced with the net spin orbital interaction energy $(\Delta e - \Delta e^0)_{\mu\mu}$.

The $\Delta e_{\mu\mu}$ values of the $(Mn_2F_{11})^{5-}$ and $(Cr_2X_{10})^{14-}$ spin dimers were calculated by using the extended Hückel method (40, 41). We used double-zeta Slater-type orbitals (42) for the d-orbitals of Mn and Cr as well as the $2s/2p$ orbitals of F, O, and S, because use of such orbitals has been found to well reproduce the trends in the antiferromagnetic spin exchange parameters of various magnetic solids (1–7).

The atomic parameters employed in our calculations are summarized in Table 3. The $\langle \Delta e \rangle$ and $\langle (\Delta e)^2 \rangle$ values calculated for the MnF_5-chain compounds are listed in Table 1, and those calculated for the CrX_2-layer compounds in Table 2. Figure 8a shows the intrachain J versus $\langle \Delta e \rangle$ plot for the MnF_5-chain systems, and Fig. 8b the corresponding J versus $\langle (\Delta e)^2 \rangle$ plot. As expected, the magnitude of J increases with increasing $\langle \Delta e \rangle$ or $\langle (\Delta e)^2 \rangle$, and both plots exhibit a reasonably good linear relationship. In particular, the compounds with four strongest spin exchange interactions (i.e., $Tl_2MnF_5 \cdot H_2O$, $Cs_2MnF_5 \cdot H_2O$, Rb_2MnF_5, and Cs_2MnF_5) are well distinguished in the two plots. However, for the two compounds with two weakest exchange interactions (i.e., Li_2MnF_5 and Na_2MnF_5), the relative magnitudes of the intrachain J values are not reproduced by the $\langle \Delta e \rangle$ or the $\langle (\Delta e)^2 \rangle$ values. The latter is understandable, because a greater error would be introduced in estimating an experimental, antiferromagnetic J in terms $\langle \Delta e \rangle$ or $\langle (\Delta e)^2 \rangle$

(i.e., in terms of J_{AF}) as the magnitude of J becomes smaller. Figure 9a shows the intralayer J versus $\langle \Delta e \rangle$ plot for the $ACrO_2$ (A = Li, Na, K, Cu, Ag) and $ACrS_2$ (A = Li, Cu, Ag) systems, and Fig. 9b the corresponding J versus $\langle (\Delta e)^2 \rangle$ plot. The correlation in the two plots is less satisfactory compared with the corresponding plots of the MnF_5-chain compounds (Figs. 8a and 8b). Nevertheless, there is a general trend that the magnitude of J decreases with decreasing $\langle \Delta e \rangle$ or $\langle (\Delta e)^2 \rangle$. It is important to note that the trends in the intralayer J values of the CrX_2 layer systems are much better reproduced by the $\langle \Delta e \rangle$ or $\langle (\Delta e)^2 \rangle$ values than by the Cr–X–Cr bridge angles.

5. CONCLUDING REMARKS

For magnetic solids with several unpaired spins per spin site, the antiferromagnetic spin exchange interactions between spin sites result largely from the diagonal terms. Thus the average quantities $\langle \Delta e \rangle$ or $\langle (\Delta e)^2 \rangle$, defined in terms of only the spin orbital interaction energies for the diagonal terms, provides a qualitative measure for the strength of antiferromagnetic spin exchange interactions in such magnetic solids. For the magnetic solids consisting of MnF_5-chains, the trends in the antiferromagnetic spin exchange interactions are well correlated with the $\langle \Delta e \rangle$ or $\langle (\Delta e)^2 \rangle$ values calculated for their spin dimers. A less satisfactory correlation is found for the magnetic solids consisting of CrX_2 layers, although the magnitude of J decreases generally with decreasing $\langle \Delta e \rangle$ or $\langle (\Delta e)^2 \rangle$. However, the trends in the intralayer J values of the CrX_2-layer systems are much better described by the $\langle \Delta e \rangle$ or $\langle (\Delta e)^2 \rangle$ values than by the Cr–X–Cr bridge angles.

ACKNOWLEDGMENTS

Work at North Carolina State University was supported by the Office of Basic Energy Sciences, Division of Materials Sciences, U.S. Department of Energy, under Grant DE-FG05-86ER45259.

REFERENCES

1. K. S. Lee, H.-J. Koo, and M.-H. Whangbo, *Inorg. Chem.* **38,** 2199 (1999).
2. H.-J. Koo and M.-H. Whangbo, *Solid State Commun.* **111,** 353 (1999).
3. M.-H. Whangbo, H.-J. Koo, and K. S. Lee, *Solid State Commun.* **114,** 27 (2000).
4. H.-J. Koo and M.-H. Whangbo, *J. Solid State Chem.* **151,** 96 (2000).
5. M.-H. Whangbo and H.-J. Koo, *Solid State Commun.* **115,** 675 (2000).
6. H.-J. Koo and M.-H. Whangbo, *J. Solid State Chem.* **153,** 263 (2000).
7. H.-J. Koo and M.-H. Whangbo, *Inorg. Chem.* **39,** 3599 (2000).
8. M. F. Charlot and O. Kahn, *Nouv. J. Chim.* **4,** 567 (1980).
9. P. Núñez, A. Tressaud, J. Darriet, P. Hagenmuller, G. Hahn, G. Frenzen, W. Massa, D. Babel, A. Boireau, and J. L. Soubeyroux, *Inorg. Chem.* **31,** 770 (1992).
10. P. Boukovec and V. Kaûcic, *Acta Crystallogr. B* **34,** 3339 (1978).
11. P. Núñez, J. Darriet, P. Boukovec, A. Tressaud, and P. Hagenmuller, *Mater. Res. Bull.* **22,** 661 (1987).
12. M. Andrés, Thesis, Univ. of Zaragoza, Spain, 1988.
13. J. Pebler, W. Massa, H. Lass, and B. Ziegler, *J. Solid State Chem.* **71,** 87 (1987).
14. A. J. Edwards, *J. Chem. Soc. A* 2653 (1971).
15. V. Kaûcic and P. Boukovec, *Acta Crystallogr. B* **34,** 3337 (1978).
16. P. Núñez and T. Roisnel, *J. Solid State Chem.* **124,** 338 (1996).
17. F. Hahn and W. Massa, *Z. Naturforsch. B* **45,** 1341 (1990).
18. D. R. Sears and J. L. Hoard, *J. Chem. Phys.* **50,** 1066 (1969).
19. S. Emori, M. Inoue, M. Kishita, and M. Kubo, *Inorg. Chem.* **8,** 1385 (1969).
20. W. Massa, *Acta Crystallogr. C* **42,** 644 (1986).
21. P. Núñez, T. Roisnel, and A. Tressaud, *Solid State Commun.* **92,** 601 (1994).
22. W. Massa and V. Burk, *Z. Anorg. Allg. Chem.* **516,** 119 (1984).
23. J. L. Soubeyroux, D. Fruchart, J. C. Marmeggi, W. J. Fitzgerald, C. Delmas, and G. Le Flem, *Phys. Stat. Sol. A* **67,** 633 (1981).
24. C. Delmas, G. Le Flem, C. Fouassier, and P. Hagenmuller, *J. Phys. Chem. Solids* **39,** 55 (1978).
25. W. Scheld and R. Hoppe, *Z. Anorg. Allg. Chem.* **568,** 151 (1989).
26. O. Croattz, F. Kubel, and H. Schmid, *J. Solid State Chem.* **122,** 247 (1996).
27. J.-P. Doumerc, A. Wichainchai, A. Ammar, M. Pouchard, and P. Hagenmuller, *Mater. Res. Bull.* **21,** 745 (1986).
28. H. Gehle and H. Sabrowsky, *Z. Naturfor. B* **30,** 659 (1977).
29. B. van Laar and D. J. W. Ijdo, *J. Solid State Chem.* **3,** 590 (1971).
30. P. Colombet and M. Danot, *Solid State Commun.* **45,** 311 (1983).
31. F. M. R. Engelsman, G. A. Wiegers, F. Jellinek, and B. van Laar, *J. Solid State Chem.* **6,** 574 (1973).
32. P. F. Bongers, C. F. Van Bruggen, J. Koopstra, W. P. F. A. M. Omloo, G. A. Wiegers, and F. Jellinek, *J. Phys. Chem. Solids* **29,** 977 (1968).
33. B. van Laar and F. M. R. Engelsman, *J. Solid State Chem.* **6,** 384 (1973).
34. P. J. Hay, J. C. Thibeault, and R. Hoffmann, *J. Am. Chem. Soc.* **97,** 4884 (1975).
35. O. Kahn and B. Briat, *J. Chem. Soc. Faraday II* **72,** 268 (1976).
36. F. Illas, I. de P.R Moreira, C. de Graaf, and V. Barone, *Theor. Chem. Acc.* **104,** 265 (2000), and the references cited therein.
37. Moreira, I. de P. R., Illas, F., Calzado, C. J., Sanz, J. F., Malrieu, J.-P., Amor, N. B., and Maynau, D., *Phys. Rev. B* **59,** 6593 (1999), and the references cited therein.
38. D. Dai and M.-H. Whangbo, in press.
39. O. Kahn, *Structure Bonding* **68,** 89 (1987).
40. R. Hoffmann, *J. Chem. Phys.* **39,** 1397 (1963).
41. Our calculations were carried out by employing the *CAESAR* program package (J. Ren, W. Liang, and M.-H. Whangbo, *Crystal and Electronic Structure Analysis Using CAESAR*, 1998. This book can be downloaded free of charge from the web site http://www.primec.com/.)
42. E. Clementi and C. Roetti, *Atomic Data Nuclear Data Tables* **14,** 177 (1974).